High Temperature Yb$_2$O$_3$-ZrO$_2$ Insulation Coatings on Ag Tapes for Magnet Technology

Mustafa KAPLAN[1], Mehmet Faruk EBEOĞLUGİL[2], Işıl BİRLİK[3], Recep YİGİT[4,5], Erdal ÇELİK[3,5,*] and Eşref AVCİ[6]

[1] Sakarya University, Engineering Faculty, Department of Metallurgical and Materials Engineering, Sakarya

[2] Dumlupinar University, Engineering Faculty, Department of Material and Ceramic Engineering, Kutahya

[3] Dokuz Eylul University, Engineering Faculty, Department of Metallurgical and Materials Engineering, Buca, Izmir

[4] Dokuz Eylul University, Izmir Vocational School, Department of Technical Programs, Buca, Izmir

[5] Dokuz Eylul University, Center for Production and Applications of Electronic Materials (EMUM), Buca, Izmir

[6] Yalova University, Engineering Faculty, Department of Chemical Processes Engineering, Yalova

* e-posta: erdal.celik@deu.edu.tr

Key words

Sol-gel; Yb$_2$O$_3$-ZrO$_2$; Insulation; Magnet technology

Abstract

In this study, synthesis and characterization of high temperature Yb$_2$O$_3$–ZrO$_2$ insulation coatings on Ag substrate were investigated for magnet technologies. The produced powders and coatings were characterized by using DTA-TG, FTIR, XRD, SEM-EDS, refractometer, spectrophotometer and empendance machines. The DTA/TG result indicates three-stage decomposition for amorphous Yb$_2$O$_3$–ZrO$_2$ composites. FTIR studies revealed that heat treated powders indicate several absoption bands corresponding to O-H, carboxyl and oxide groups. Though ZrO$_2$ phase present in the structures with high intensity, Yb$_3$O$_2$ phase possessess low intensity peak. A regular surface morphology generally forms once Yb$_2$O$_3$ content increase in ZrO$_2$ from 0 mole % to 12 mole %. The refractive indexes of Yb$_2$O$_3$–ZrO$_2$ coatings were found to be in the range of 1.3539 and 1.3655. The film thicknesses of all coatings generally increased from 0.50 µm to 1.20 µm according to number of dipping. Optical band gap values of Yb$_2$O$_3$–ZrO$_2$ coatings are approximately 3,014 eV. Empedance values of ZrO$_2$ and Yb$_2$O$_3$-ZrO$_2$ coatings were measured as 2.52 ohms and 2.51 ohms, respectively.

Mıknatıs Teknolojisi İçin Ag Şeritler Üzerindeki Yüksek Sıcaklık Yb$_2$O$_3$-ZrO$_2$ Yalıtkan Kaplamalar

Anahtar kelimeler

Sol-jel; Yb$_2$O$_3$-ZrO$_2$; Yalıtkan; Mıknatıs teknolojisi

Özet

Bu çalışmada, mıknatıs teknolojileri için Ag altlık üzerinde yüksek sıcaklık Yb$_2$O$_3$–ZrO$_2$ yalıtkan kaplamaların sentezlenmesi ve karakterizasyonu incelenmiştir. Üretilen tozlar ve kaplamalar DTA-TG, FTIR, XRD, SEM-EDS, refraktometre, spektrofotometre ve empedans cihazları kullanılarak karakterize edilmiştir. DTA-TG sonucu amorf Yb$_2$O$_3$–ZrO$_2$ kompoziti üç kademeli bozunma göstermiştir. FTIR çalışmaları ısıl işlem yapılmış tozların O-H, karboksil ve oksit gruplara tekabül eden çeşitli absorbsiyon bandlarını içerdiğini açıklamıştır. Kaplama yapısında ZrO$_2$ fazı yüksek şiddette olmasına rağmen, Yb$_3$O$_2$ fazı düşük şiddete sahiptir. ZrO$_2$'daki Yb$_2$O$_3$ içeriği % 0 molden % 12 mole artırıldığında, genellikle düzenli yüzey morfolojisi oluşmuştur. Yb$_2$O$_3$–ZrO$_2$ kaplamaların refraktif indeksi 1.3539 ve 1.3655 aralığında bulunmuştur. Tüm kaplamaların kalınlıkları daldırma sayılarına göre 0.50 µm'den 1.20 µm'e değişmiştir. Yb$_2$O$_3$–ZrO$_2$ kaplamaların optik enerji aralığı yaklaşık olarak 3,014 eV'dir. ZrO$_2$ ve Yb$_2$O$_3$-ZrO$_2$ kaplamaların empedans değerleri sırasıyla 2.52 ohm ve 2.51 ohm olarak ölçülmüştür.

1. Introduction

New types of high temperature ZrO$_2$-based ceramic insulation on long-lengths of Ag and AgMg sheathed Bi$_2$Sr$_2$CaCu$_2$O$_{8+\delta}$ (Bi-2212) and Bi$_2$Sr$_2$Ca$_2$Cu$_3$O$_{8+\delta}$ (Bi-2223) tapes and wires have been developed through a reel-to-reel, continuous sol–gel technique in order to provide turn-to-turn electrical insulation for high temperature superconducting (HTS) coils applications (Mutlu, *et. al.* 2002). For this application, effectiveness of insulation materials is a very important parameter in minimizing the leaks and resistance to reactions during the partial melt texturing process. To

provide these, ZrO$_2$, MgO–ZrO$_2$, Y$_2$O$_3$–ZrO$_2$, CeO$_2$–ZrO$_2$, Sm$_2$O$_3$–ZrO$_2$, Ho$_2$O$_3$–ZrO$_2$, Er$_2$O$_3$–ZrO$_2$, Gd$_2$O$_3$–ZrO$_2$, Tb$_2$O$_3$–ZrO$_2$, In$_2$O$_3$–ZrO$_2$, and SnO$_2$–ZrO$_2$ coatings were developed and used to insulate Ag and AgMg/Bi-2212 tapes. Such insulation coatings are compatible with high processing temperatures, for instance partial melt texturing of AgMg/Bi-2212 about 900 °C for 20 hours in air, and low operation temperature 4.2 K (Weijers, *et. al.* 2000; Celik *et.al.* 2003; Celik *et.al.* 2002; Celik *et.al.* 2002; Celik, 2010). Of these insulation coatings, Yb$_2$O$_3$–ZrO$_2$ has not yet published in literature for magnet technologies. In present research, high temperature 0 %, 5 %, 8 % and 12 mole % Yb$_2$O$_3$–ZrO$_2$ insulation coatings deposited on Ag tape substrates from solutions of zirconium tetrabutoxide, Yb 2, 4-pentanedionate, methanol and glacial acetic acid via sol-gel technique as a new material.

2. Material and Method

The solutions utilized in the coatings were separately prepared from Yb and Zr based precursor materials. Now that commercial chemical materials are not always pure when purchasing from any company, purity of precursors was checked with titration method before preparing solutions. Yb 2, 4 pentanedionate (Yb(CH$_3$COCHCOCH$_3$)$_3$, 99.9%) chemical powders with different concentrations were dissolved in methanol which is used as a solvent and consequently Zr tetrabutoxide (Zr(O(CH$_2$)$_3$CH$_3$)$_4$, 99.9%) liquid matrix was added to the prepared solution as a second precursor. An adequate amount of glacial acetic acid was also mixed to the solutions in order to act as a stabilizing agent by forming a chelate complex. In this research, amount of Yb$_2$O$_3$ in the insulation was chosen as 0 %, 5 %, 8 % and 12 mole % by calculating as mole percentages to stabilize ZrO$_2$. The final solutions were formed through the hydrolysis of Zr and Yb alkoxides after vigorously stirring at room temperature for a 1 hour period at 100 rpm. After hydrolysis process, the resultant solutions were clear and stable at room temperature in air. Transparent solutions, which are completely

dissolved from powder precursors, can remain at least 30 days without precipitation. The clear, yellowish and transparent solutions resulted with no visible particles reflecting the polymeric nature of the sol species.

Turbidity measurements of the prepared solutions were performed at room temperature with help of "TB 1 turbidimeter velp scientifica" called machine. Transparency of the solutions was determined by the machine. The pH values of the prepared solutions were measured using a standard pH meter with Mettler Tolede electrode. In these measurements, the determination of gelling and long-term stabilization processes of the prepared solutions can be anticipated to be utilized in the insulation method before coating technique. The highly stabilized transparent solutions can provide cost-effectiveness, good wettability, film quality and mechanical properties, as well as offering advantages in long-term usage performance as a liquid form. This makes it easy to use in coating process and meets the reqiurements of the insulation materials within magnet technologies.

Commercial highly pure Ag tapes with nominal dimensions of 65 mm x 0.0125 mm x 7 mm were utilized as substrates inasmuch as Ag-based materials ideally are used as sheathing elements in Bi-2212 and Bi-2223 superconductors via Powder-In-Tube (PIT) technique. The substrate was cleaned with acetone before coating process in order to eliminate dirtiness on the surface. The solutions were deposited on both sides of the substrates by using a dip coating process with a withdrawal speed of 0.3 cm/sec and with a dwell time inside the solution for 3 min at room temperature in air. After dipping process, the obtained gel coatings were dried at 300 ^{o}C for 10 minutes, heat treated at 500 ^{o}C for 5 minutes and subsequently annealed at 800 ^{o}C for 1 hour in air. Thicker coatings were obtained by repeating this process over and over again before annealing process and also by increasing viscosity of solution. Hence, number of dipping varied between 6 and 10 times for coating process.

Thermal behavior of Zr- and Yb-based xerogels, which were heat treated at 150 ^{o}C for 30 minutes in air after drying at room temperature for 24 hours, was scrutinized from room temperature upto 850 ^{o}C at a heating rate of 10 °C/min under oxygen atmosphere by using differential thermal analysis-thermograviometry (DTA-TG) machine (DTG-60H Shimadzu) in order to gain decomposition and phase formation, and to obtain an optimum heat treatment regime for drying, heat treatment and annealing processes. Prior to performing DTA-TG measurement of the xerogels, they were weighted as approximately 20 mg and then put into crucible. Fourier transform infrared spectroscopy (FTIR) analysis of dried gels and calcined powders were carried out in an Perkin Elmer spectrometer in the wavelength range of 4000 to 400 cm^{-1} at 25 ^{o}C in order to determine chemical groups of the samples heat treated at 100 ^{o}C, 300 ^{o}C, 500 ^{o}C and 800 ^{o}C for 30 min in air at intermediate temperatures in insulation coating production.

For phase analysis, X-ray diffractometry (XRD) studies of Yb$_2$O$_3$–ZrO$_2$ insulation coatings were performed through Rigaku (D/MAX-2200/PC) diffractometer with a CuK$_\alpha$ irradiation (wavelength, λ=0.15418 nm). Thin-film XRD geometry where incident angle was fixed at 1° was used to collect data from thin films. The surface morphologies and elemental analyses of Yb$_2$O$_3$–ZrO$_2$ coatings were carried out by means of scanning electron microscopy (SEM, JEOL JSM 6060) including energy dispersive spectroscopy (EDS).

Refractive index, coating thickness and optical band gap of the insulated coatings on glass substrates were evaluated using refractometer and spectrophotometer machines. Notwithstanding Ag substrate was normally used in the experiments, glass substrates were coated to measure their refractive index, coating thickness and optical band gap values. Refractive indexes of the coatings were measured at selected wavelengths in the VIS region by a high-accuracy Abbe refractometer at room temperature. Refractive indexes were used to

determine coating thickness and optical band gap using V-530 JASCO UV/VIS Spectrophotometer and Abbe refractometer, respectively. As for optical band gap of the coatings on glass substrates, it is well known that in an amorphous material like glass characterized by indirect allowed transitions, the absorption coefficient varies with the photons energy according to the Tauc's relation (Ech-chamikh *et.al.* 2006):

$$\sqrt{\alpha h \nu} = B(h\nu - E_{opt}) \qquad (1)$$

where ν is the frequency of incident photons, E_{opt} the optical gap, h the Planck's constant and B a constant. The variation of $(\alpha h \nu)^{1/2}$ as a function of the energy $h\nu$ shows a linear behavior near the band gap. The value of the energy band gap is given by the intercept of the straight line with the energy axis. Moreover, transmittance and absorbance properties of the coatings on glass substrate by V-530 JASCO UV/VIS Spectrophotometer with a blank piece of substrate in the reference beam.

Dielectrical properties of the insulated coatings were determined using Novocontrol Alpha-N High Resolution Dielectric Analyzer. With regard to dielectric characteristics of the insulation coatings, relevant tests are conducted at room temperature. In this context, empedance and conductivity of the insulation coatings were measured as dielectric characteristics. Since sample cells were utilized as a plate capacitor, the sample material was placed between two external capacitor plates. For the measurements, frequency range is taken between 10^{-3} and 10^7 Hz.

3. Results and Discussion

3.1. Solution properties

Turbidity is of prime concern to consider further processess as to giving clues involving drying, annealing, homogeneous films, mechanical and electrical properties. Turbidity which means the relative cloudiness of a liquid gives the optical characteristic of suspense particles in a liquid. Ligth is passed through the sample and is scattered in all directions. The light that is scattered at 90° angle to

the incident light is then dedected by a photodiode and is converted into a signal linearized by analyzer and displayed as ntu. The more suspended particles there are in a liquid, the more light will be scattered, resulting in a higher ntu value (Wilde and Gibs). With turbidity experiments, whether powder based precursors in the solutions are dissolved very well is understood as ntu values before coating process. Note that the measurement range is between 0 ntu and 1000 ntu. It is interpreted that powder based precursors is completely dissolved as turbidity value approaches to 0 ntu. On the other hand, they are not dissolved and some powder particles are suspended in a solution as it approaches to 1000 ntu. Worth nothing here is that the fabrication of homogeneous, continuous and thin film depends directly on turbidity value which is 0 ntu. Turbidity values of the prepared Zr-based and Yb, Zr-based solutions are listed in Table 1. Turbidity values of Yb and Zr-based solutions including 0, 5, 8 and 12 % mole Yb were found to be 12.42, 4.24, 31.02 and 62.81 ntu, respectively. It is obviously clear from these results that turbidity is affected by Yb concentration in the solutions. When Yb content in the solution was increased, its turbidity values increased. Owing to these results, it can be recommendable for the further processing. More importantly, it can be stated out that that the recommended level in the turbidity values indicate that the solutions are clear and transparent at room temperature.

Table 1. Turbidity and pH values of the prepared solutions

Solutions	Turbidity (ntu)	pH
0% Yb$_2$O$_3$-ZrO$_2$	12.42	4.05
5% Yb$_2$O$_3$-ZrO$_2$	4.24	2,81
8% Yb$_2$O$_3$-ZrO$_2$	31.02	2,97
12% Yb$_2$O$_3$-ZrO$_2$	62.81	2,82

The sol–gel process involves the hydrolysis of an alkoxide or salt precursors under acidic or basic conditions, followed by polycondensation of the hydroxylated monomers to form a porous gel network. After that, gel aging and drying can be conducted to obtain densified solid matrices. The rate, extent and even the mechanism of the reaction are profoundly influenced and may be controlled by many factors such as pH, water:alkoxide ratio (R), type of catalyst, solvent and precursor, as reported in literature (Jerónimo, *et. al.* 2004) in details. The pH value of solutions strongly depends on these factors. In this study, we exclusively found that the functional dependence is essentially identical to that seen at these applications, showing that transparent solutions were obtained by preparing with strong acidic conditions thereby concentrations of solvent and chelating agent was remained at a constant concentration but Yb content was increased in the solution. According to these results, the pH values of the solutions were determined to be in the range of 2.81 and 4.05 as listed in Table 1. Hydrolysis/chelation time of the solutions can be anticipated after their stabilization using pH meter. When the solution came to stabilization, hydrolysis and gelation are completed as below:

Hydrolysis;
$$M(OR)_x + H_2O \rightarrow H\text{-}O\text{-}M(OR)_{x-1}(OH) + ROH \qquad (2)$$

Chelation;
$$M(OR)_x + HOOAc \rightarrow M(OR)_{x-y}(OAc)_y + ROH \qquad (3)$$
where; M: Zr and Yb.

3.2. DTA-TG analysis

Proper choice of temperature, time and atmosphere for process optimization in sol-gel process depends on thermal stability of the insulation coatings at high temperatures (800 ^{o}C) and the decomposition of carbon based materials at low temperatures (100-400 ^{o}C). By this way, thermal behaviors of Zr-based and Yb and Zr-based xerogels dried at 150 ^{o}C for 30 minutes in air was denoted in Figure 1. It is clear from Figure 1 that there exist three thermal phenomena such as solvent removal, combustion of carbon based materials and oxidation which promotes process optimization. These kinds of thermal phenomena can be seen in all sol-gel process. DTA curves of both samples revealed that endothermic and

exothermic reactions occurred at temperatures between 30 °C and 500 °C. It was due to the fact that physical water and solvent evaporated and also carbon based materials coming from alkoxides, solvent and chelating agent burnt out in the xerogel samples. The first thermal phenomenon of Zr-based and Yb and Zr-based xerogels was the solvent removal in the temperature ranges of approximately 80-90°C and 50-175°C, respectively. The initial step during heat treatment process of the insulation is associated with the evoparation of solvent in the gel structure bearing hydroxyl group in the presence of the increasing temperature in a real application. At these temperatures, the endothermic reaction is mostly due to evaporation of volatile e organic components. The peak Yb and Zr-based xerogel samples were found to be temperatures of solvent removal for Zr-based and approximately 85°C and 98°C, respectively. The second phenomenon of Zr based and Yb, Zr based xerogel samples was combustion of OR groups at temperature ranges 200-320°C and 175-300°C, respectively. Large exothermic peaks were determined at these temperature ranges in terms of combustion of carbon based materials. In that literature reviewed says the same phenomena, we have a good agreement with a research of Yue et. al. (2004), showing that the oxygen can accelerate the combustion process and a great amount of the heat generates in this exothermic reaction. This results in violent combustion because of this reason. The last stage was the formation of ceramic oxides between 430 and 420°C for both samples. The maximum oxidation temperatures of Zr-based and Tb and Zr-based samples were found to be approximately 500°C and 450°C, respectively. When Zr-based and Zr- and Yb- based xerogels are heated up from room temperature to 800°C, $Zr[O(CH_2)_3CH_3]_4$, $Yb(CH_3COCHCOCH_3)_3$, CH_3COOH and CH_3OH components are oxidized at temperatures between 200 and 550°C as follows:
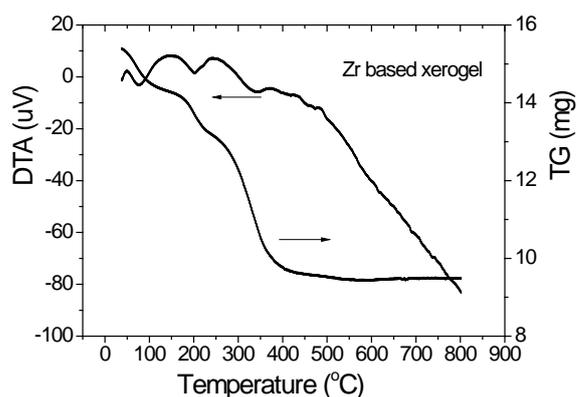
(a)
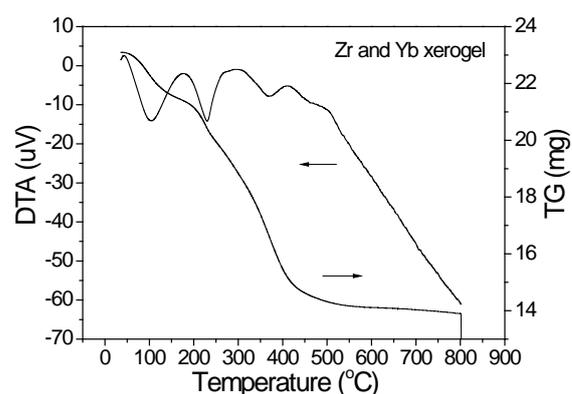
(b)

Figure 1. DTA and TG curves of (a) pure Zr-based and (b) Zr, Yb-based xerogels dried at 150°C for 30 minutes in air as a function of temperature

$$Zr[O(CH_2)_3CH_3]_4 + 24O_2 \rightarrow ZrO_2 + 16CO_2 + 18H_2O \quad (4)$$

$$2Yb(CH_3COCHCOCH_3)_3 + 36O_2 \rightarrow Yb_2O_3 + 30CO_2 + 21H_2O \quad (5)$$

$$CH_3OH + O_2 \rightarrow CO + 2H_2O \quad (6)$$

$$CH_3COOH + O_2 \rightarrow 2CO + 2H_2O \quad (7)$$
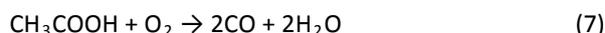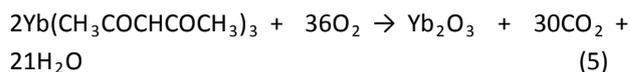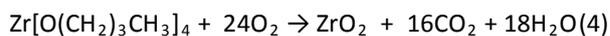
in which, Yb₂O₃–ZrO₂ ceramic oxide is formed at these temperatures. Methanol and glacial acetic acid are converted to CO₂/CO and H₂O gases in terms of heating process.

Based on the investigated TG curves in Figure 1, the observed weight loss values of pure Zr-based and Yb, Zr-based xerogel powders for oxidation reactions were determined to be ~55 % and ~40 %, respectively and it is in progress until approximately 550 °C. As seen from TG curve, maximum amounts of weight lost were occurred during combustion of carbon based materials. The slope of TG curves decreases quickly when carbon

based materials burn out from the samples. Analysing TG curves of both samples shows that a 0.5-1 % mass reduction occurs between 25 and 200°C due to solvent elimination. Between 200 and 400° C an exothermic process takes place with 35 % and 21 % mass reductions due to the decomposition of the organic components for pure Zr-based and Yb, Zr-based xerogel powders, respectively. All observed weight loss values agrees well with all transformations. The outstanding findings have emerged from these results, indicating that an optimum heating regime for this process was eventually determined at temperatures such as 300°C for 10 minutes, 500°C for 5 minutes and 800°C for 60 minutes which respectively indicate combustion or drying, oxidation or heat treatment and annealing processes.

3.2. FTIR analysis

FTIR analysis is a very sensitive and well-established tool for studying the transformation and nature of bonds in both Zr-based and Zr- and Yb-powders heat-treated at different temperatures corresponding to exothermic and endothermic peaks in DTA-TG results, Therefore, the FTIR results could well be correlated with the crystallization behavior and phase evolution in the gels as well as calcined powders in ZrO$_2$ and Yb$_2$O$_3$–ZrO$_2$ coating systems. Dependent on these behaviors, FTIR results are valuable for these analyses. Figure 2 denotes FTIR absorbance spectra of Zr-based and Yb, Zr-based powders which were heat treated at 100 ^{o}C, 300 ^{o}C, 500 ^{o}C and 800 ^{o}C for 30 minutes in air for all chemical compositions. FTIR spectra of the obtained powders were examined to investigate the chemical and structural changes that take place during heat treatment process. The major peaks appearing in the FTIR spectra of Zr-based and Yb, Zr-based powder systems could be related to the following: (1) –OH stretching vibration of the surface bonded water; (2) –OH bending vibration of the surface bonded water; (3) –OH stretching vibration of structural water, corresponding to M–OH bonding; (4) –OH bending vibration of structural water, corresponding to M–

OH bonding; (5) C-H stretching vibration of organic group, corresponding to CH$_2$ and CH$_3$ bonding; (6) C=O stretching vibration of organic group, bridging type metal-acetate bonding (M-OCOO-M); (7) Zr–O stretching vibration; and (8) Yb–O stretching vibration. As may be expected from here, both samples exhibited similar behaviors. Additionally, FTIR structure of zirconium (IV) acetylacetonate exhibited a similar absorbance band with that of Zr-based and Yb, Zr-based powders heat treated at different temperatures. It is clearly seen from Figure 2 that the heat treated powders demonstrate several absoption bands at about 3300-3700 cm^{-1}, 2400-2700 cm^{-1}, 1400-1800 cm^{-1}, 900 cm^{-1} and 500 cm^{-1} corresponding to O-H, carboxyl and oxide groups. A broad band located around 3500 cm^{-1} is in the typical range for the OH$^-$-stretching mode absorptions both samples at 100°C and 300°C. On the other hand, the bands at 3300 and 3700 cm^{-1} are due to O-H species in the Yb- and Zr-based xerogel which was heat treated at 25°C and 300°C, respectively and those at 2400-2700 cm^{-1} are due to C-H stretching frequencies. For example, the presence of CH$_2$ and CH$_3$ organic

(a)

(b)
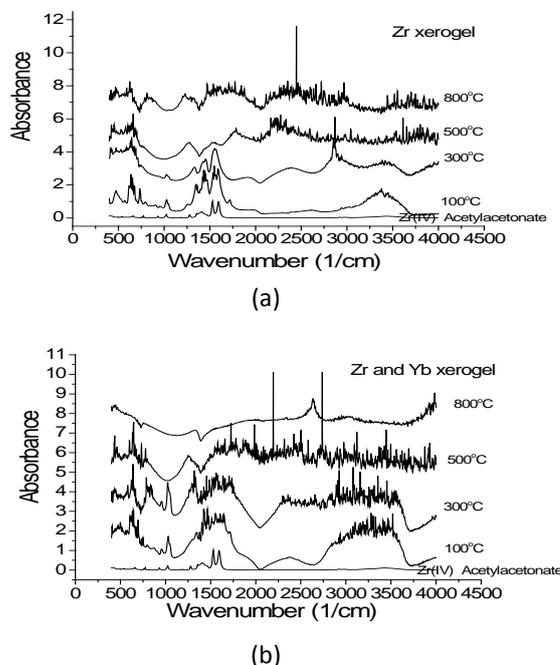
Figure 2. FTIR absorbance spectra of (a) Zr-based and (b) Yb, Zr-based powders heat treated at 100 ^{o}C, 300 ^{o}C, 500 ^{o}C and 800 ^{o}C for 30 minutes in air

groups was monitored through their vibrational modes occurring in the 2200–3800 cm^{-1} range. The

band seen in the range of 1400 and 1800 cm^{-1} is due to C=O arising owing to bridging type metal-acetate bonding (M-OCOO-M). It should be remarked that by using the weaker acetic acid the absorption spectra were practically independent of the amount of the acid in the starting solution. The spectra of the samples which were heat treated at 25°C and 300°C were nearly similar. Nonetheless, the OH band has shifted slightly towards lower frequencies as seen in Figure 2. When increasing heat treatment temperature from 25°C to 800°C, the frequencies of O-H, C-H, and C=O bands decreased. The spectrum of Yb₂O₃–ZrO₂ precursor film heat treated at 500°C and 800°C denotes an absence of absorption bands corresponding to organics and hydroxyls indicating complete removal of organics and hydroxyls. Moreover, the common features that appear below 900 cm^{-1} corresponds to the stretching vibrations of Zr=O and Yb=O and also to the contributions of Zr-O and Yb-O or Yb-O-Zr bonds. In the spectrum of 500°C and 800 °C, the band at ≈ 500 cm^{-1} may be assigned to the vibration of ZrO₂ and Yb₂O₃ bands appear at high temperatures. On the other hand, it is believed that the features particularly at 500 cm^{-1} and 900 cm^{-1}, due to Zr–O₂–Zr and Yb-O₂-Yb asymmetric and Zr–O and Yb-O stretching modes respectively, confirm the formation of ZrO₂ and Yb₂O₃ phases. The difference in Yb₂O₃–ZrO₂ sample was clearly seen in the band at ≈500 cm^{-1}.

3.3. Phase structure

The phase identification of 0, 5, 8 and 12 mole % Yb₂O₃–ZrO₂ coatings on Ag tapes was performed in favor of XRD after annealing process at 800°C for 1 hour in air. The XRD spectra of the insulated coatings shown in Figure 3 obtained by Rigaku diffractometer in the 2-θ range 5–90°. It can be noticed that sol–gel technique produces pure fluorite-type ZrO₂ and Yb₂O₃–ZrO₂ at 500 °C as while conventional solid-state reaction methods in which processing temperature around 1400 °C is usually required for single-phase and stabilized materials (Celik, *et.al.* 2004). XRD patterns revealed that whilst ZrO₂ phase present in the structures with high intensity, Yb₃O₂ phase has low intensity

peak. Once increasing the amount of Yb₃O₂ in ZrO₂ coating, intensity of Yb₂O₃ phase increased. The XRD results also suggest that the structure of the ZrO₂ and Yb₂O₃–ZrO₂ coatings are polycrystalline phases with monoclinic and tetragonal structures. Diffraction peaks originated from planes of monoclinic ZrO₂ were indexed as *m(h k l)* in pure ZrO₂ coatings, while diffraction peaks originated from planes of tetragonal ZrO₂ were indexed as *t(h k l).* The three peaks at 2θ=28.3°, 30.1° and 31.4°, indexed as $m(11\bar{1})$, *t(1 0 0)* and *m(1 1 1),* respectively, were used to identify tetragonal and monoclinic ZrO₂ phase (Celik 2010). As a comparison, only one peak from tetragonal ZrO₂ appears in patterns of Yb₂O₃–ZrO₂ coatings annealed at 800°C for 1 hour in air. More importantly, as it was expected, no peaks originated from monoclinic phase are observed for Yb₂O₃-ZrO₂ coatings annealed at 800 °C, which is good temperature for insulation process. The Yb₂O₃ peak at 2θ=14° was clearly seen from Yb₂O₃-ZrO₂ coatings on Ag substrate. The intensity of Yb₂O₃ peak increased with increasing its content in the coatings. In process optimisation, XRD analyses strongly supported to determine annealing temperature with a combination of DTA-TG and FTIR results. Therefore, current work is endevouring to optimize process for high temperature insulation coatings, specifically Yb₂O₃-ZrO₂, with contribution of DTA-TG, FTIR and XRD results.
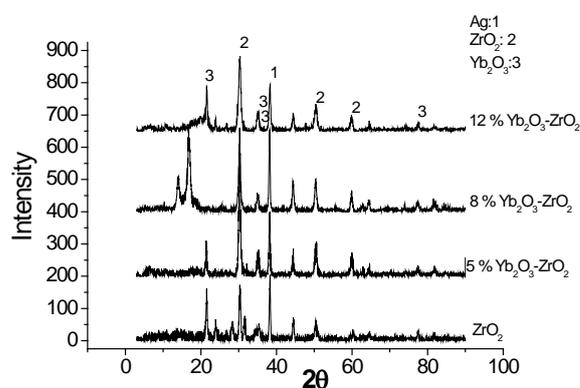
Figure 3. XRD patterns of ZrO₂ and Yb₂O₃–ZrO₂ coatings on Ag tape substrates.

3.4. Microstructure

Figures 4 and 5 shows SEM micrographs and X-ray maps of 0 %, 5 %, 8 % and 12 mole % Yb$_2$O$_3$-ZrO$_2$ coatings on Ag tapes. As presented from microstructural observations, a regular surface morphology generally forms when Yb$_2$O$_3$ content increase in ZrO$_2$ from 0 mole % to 12 mole %. In Figure 4.a, it can be easily seen that homogenous structure forms in pure ZrO$_2$ coatings with islands. The average size of the coating island was found to be 10 µm in the coating. However, coating islands sligthly altered in 5 %, 8 % and 12 mole % Yb$_2$O$_3$-ZrO$_2$ coatings as size. In Figures 4.b, 4.c and 4.d, the sizes of coating islands were determined in the range of 10 and 40 µm. It is interesting to state out here that these coatings with mosaic structure are obtained for the coatings which applied six cycles on Ag substrates. These structures can be seen in
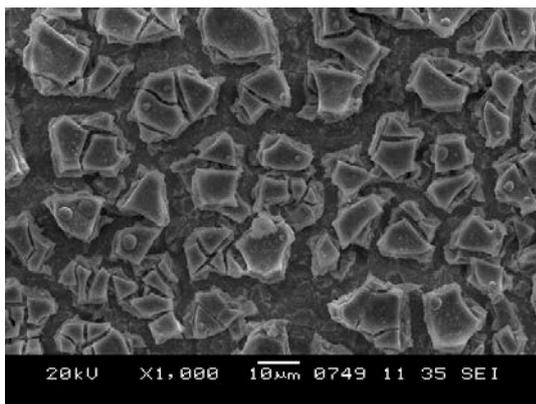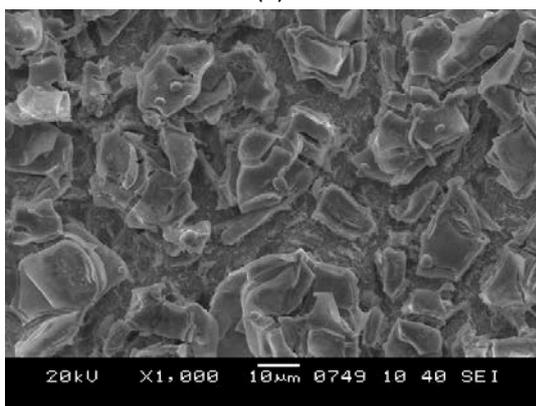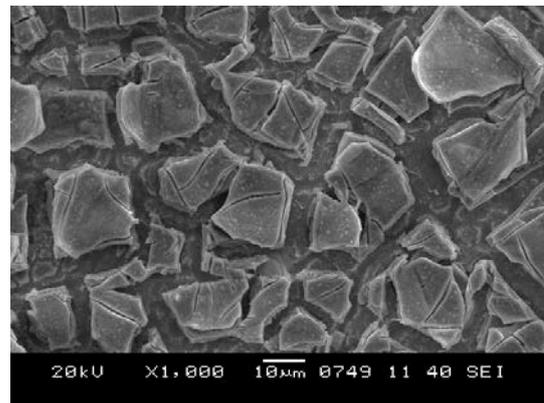
(c)
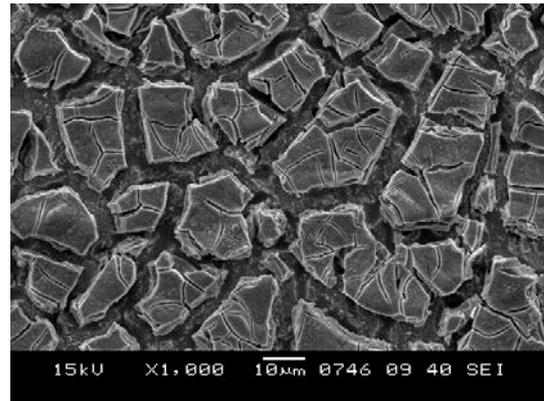
(d)

Figure 4. SEM microstructures of (a) 0, (b) 5, (c) 8 and (d) 12 mole % Yb$_2$O$_3$–ZrO$_2$ coatings on Ag substrates after heat treatment. The scale bars are 10 µm for all coatings

(a)

(a)

(b)
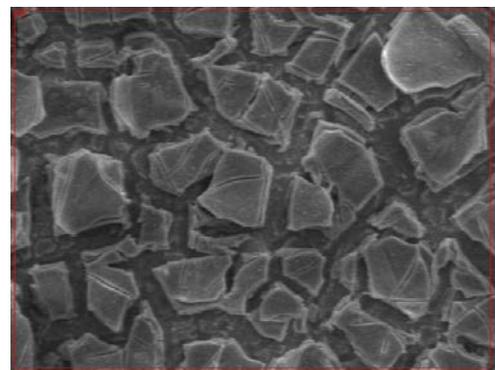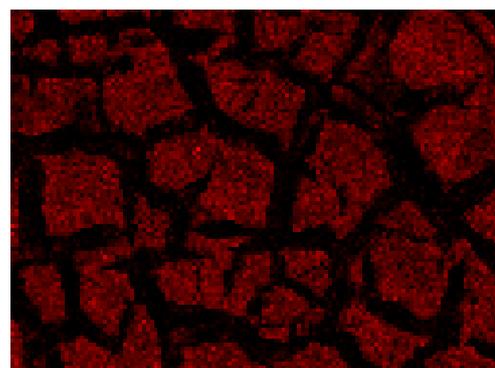
(b)
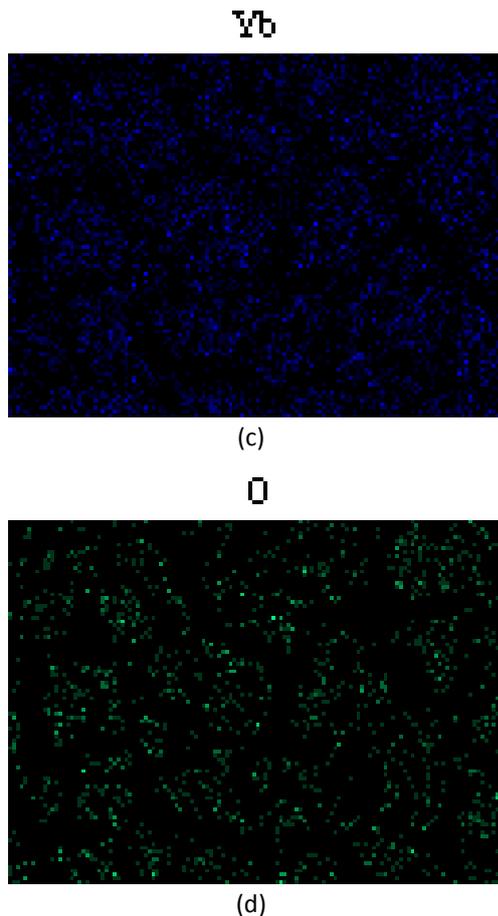
Figure 5. (a) SEM microstructure and (b, c, d) X-ray maps of Yb$_2$O$_3$-ZrO$_2$ coatings obtained on Ag substrates after heat treatment. X-ray maps were taken from (a), and (b) Zr, (c) Yb and (d) O maps were obtained from Yb$_2$O$_3$-ZrO$_2$ coating (a).

all sol-gel derived coatings because of heat treatment and annealing processes. In 5 mole % Yb$_2$O$_3$-ZrO$_2$ coatings, homogeneous and regular islands are formed as seen Figure 4.b., but this structure is slightly different from other coatings. As for 8 mole % Yb$_2$O$_3$-ZrO$_2$ coatings (Figure 5.c), bigger grains formed in state of coating islands resulted in micro cracks with process propagation. When looking at surface of 12 mole % Yb$_2$O$_3$-ZrO$_2$ coatings (Figure 4.d), it can be seen that microcracks and small domes formed during the process. Generally speaking, the coating coverage on the substrate is very good. This kind of structure is understandable from the fact that the nano-crystals of Yb$_2$O$_3$-ZrO$_2$ formed at high temperatures tend to be highly crystalline in nature and defect free. Nevertheless, because annealing procedure of the insulations was performed at

800°C, some inhomogenities were observed in Yb$_2$O$_3$-ZrO$_2$ coatings. The film thickness and surface defects increase in accordance with the same number of layers. Minimum coating thickness was obtained while decreasing number of dipping and structural observation of minimum thickness samples possesses the required properties. In addition to these points, in terms of the application of thermal processes carried out at high temperatures some cracks result inside the coating. Note that the cracks in coating resembles coating island on substrate. Inasmuch as viscosity, withdrawal speed, surface tension and contact angle with substrate are very important factors in sol-gel processing, surface morphology and mechanical properties of coatings are strongly affected from these parameters. The thickness of sol–gel coatings is controlled by several factors, including withdrawal rate and solution viscosity. Under the condition of constant withdrawal rate, viscosity can be regarded as the dominant parameter in establishing the final coating thickness. The viscosity of a solution containing Zr based precursor increases non-linearly. It was observed that more compact coatings were obtained on Ag tapes after annealing, which was carried out at a temperature of 800 °C under a flowing oxygen atmosphere. As expected, the temperature provides a densification of the coatings during this process.

In this application, it can be seen at first glance as a major improvement with respect to the insulation coatings of the Ag/AgMg tapes. However, the requirement is to produce the insulation coatings with cracks, on account of the fact that Bi-2212 phase is formed at annealing conditions because oxygen gas in the furnace is needed to react with superconducting ceramic materials in Ag/AgMg tapes, and also that thermal shock of the insulation coatings is prevented at high sintering temperature (800 °C for 20 h) and low cryogenic temperature (4.5 K and liquid He). The W&R process is also one of the reasons. In W&R process, an electromagnet is fabricated by winding the tapes and reacting at approximately 800 °C for 20 h in oxygen

atmosphere. While winding process, an excessive stress concentration and a failure can easily form if there are no cracks in the coating. On the contrary, a failure can prevent in the electromagnet if there are cracks in the coatings. Because of these reasons, cracks strongly want to possess in coating structure. With the insulation process of the HTS conductors before winding using the reel-to-reel sol–gel method, the oxidation of the Ag/AgMg sheathing tapes is prevented during W&R technique. In this method, the insulated conductors are wound to fabricate coils and double pancakes. These coils are annealed at around 800 °C for several hours under flowing oxygen atmosphere in tube-furnaces with both the coil and the furnace axis horizontal. It can be pointed that sol–gel ZrO$_2$ and Yb$_2$O$_3$-ZrO$_2$ insulation coatings having crack are fully compatible with Ag/AgMg sheathed Bi-2212 superconducting tape substrates by virtue of oxygen permeability, high and low actual temperatures and the W&R process in comparison with the conventional insulation process.

One of the characterizations associated with the insulation coatings is the elemental mapping analysis, which limits investigation of these materials to a laboratory scale. With the homogeneous distribution attention of Zr, Yb and O elements in the coatings, it is a significant issue to verify that the elemental maps of the insulation coatings on Ag substrate. In the microstructural observations, a slight difference in microstructures of the coatings can be seen easily in Figure 5. It is believed that this difference results in Yb$_2$O$_3$ content in the coatings. X-ray maps of Zr, Yb and O atoms in the coatings were obviously indicated in Figure 5, exhibiting that these elements also possess a regular distribution.

3.5. Refractive index, coating thickness and optical band gap

Even though Yb$_2$O$_3$–ZrO$_2$ based coatings are not optical materials, we deal notably with how to measure coating thickness and optical band gap of the coatings using refractive index measurements. As far as the insulation coatings used in HTS

applications are concerned, the coating thickness is generally required to be accurately controlled. Otherwise the prepared insulation coatings will not serve as well as those which have been designed in advance. However, nowadays the properties of the insulation coatings are directly related to the thickness of the final solid films. In this context, the film thickness of Yb$_2$O$_3$–ZrO$_2$ based coatings were calculated according to the number of dipping by using measured refractive indexes. Refractive index, coating thickness and optical band gap values of the insulating coatings were listed in Table 2. In this sense, the refractive indexes of 0 %, 5 %, 8 % and 12 mole % Yb$_2$O$_3$–ZrO$_2$ coatings annealed at 800°C were found in the range of 1.3539 and 1.3655. Using these values, it was determined that the film thicknesses of all coatings generally increased from 0.50 μm to 1.20 μm with increasing with number of dipping from 1 layer to 6 layers. Depending on these, the coating thicknesses of 0 %, 5 %, 8 % and 12 mole % Yb$_2$O$_3$–ZrO$_2$ coatings annealed at 800°C were determined to be approximately 1.20 μm for 6 layers. As for optical band gap values of 0 %, 5 %, 8 % and 12 mole % Yb$_2$O$_3$–ZrO$_2$ coatings annealed at 800°C, they are found to be 3,0036 eV, 3,05166 eV, 3,02133 eV and 3,02836 eV, respectively. From these results, it was not seen a remarkable rise in the energy gap values in the insulation coatings. Actually, it is evidence that there is a relationship among the insulation coatings.

Table 2. Thicknesses, refractive indexes and band gap values of ZrO$_2$ and Yb$_2$O$_3$-ZrO$_2$ insulation coatings on glass substrates

Coatings	Thickness (μm)	Refractive index (nD)	Energy gap (eV)
0% Yb$_2$O$_3$-ZrO$_2$	1.219	1.3606	3,00366
5% Yb$_2$O$_3$-ZrO$_2$	1.152	1.3655	3,05166
8% Yb$_2$O$_3$-ZrO$_2$	1.076	1.3539	3,02133
12% Yb$_2$O$_3$-ZrO$_2$	1.356	1.3572	3,02836

3.6. Dielectric properties

Figure 6 denotes empedance and conductivity curves of ZrO$_2$ and Yb$_2$O$_3$-ZrO$_2$ coatings on Ag tape substrates as a function of frequency. As indicated beforehand, frequency range was taken between

10^{-3} and 10^7 Hz. In insulative coating system, empedance and conductivity are important factors in two wound tapes. In this research, empedance

(a)

(b)
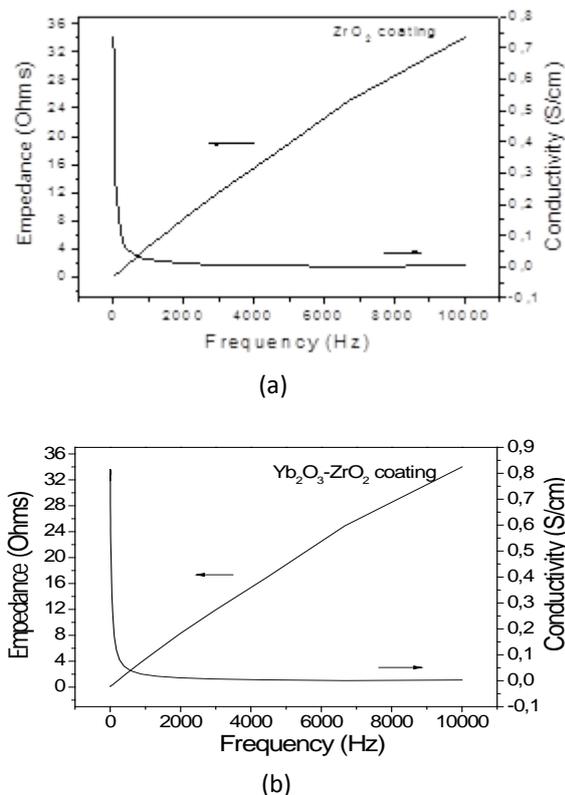
Figure 6. Empedance and conductivity versus frequency curves for (a) ZrO_2 and (b) Yb_2O_3-ZrO_2 insulation coatings on Ag substrate

values of ZrO_2 and Yb_2O_3-ZrO_2 coatings were measured as 2.52 ohms and 2.51 ohms, respectively. Similarly conductivity values of ZrO_2 and Yb_2O_3-ZrO_2 coatings were found to be 0.488 S/cm and 0.550 S/cm, respectively. When Yb_2O_3 was added to ZrO_2 coatings, their empedance did not change from low values to high ones considerably. Due to these reasons, after both sides of commercial Ag and AgMg sheathed Bi-2212 long length tapes are insulated with pure ZrO_2 and Yb_2O_3–ZrO_2 coatings, it can be wound to fabricate an electromagnet. In this application, high temperature insulation coatings do not directly influence superconducting properties, but prevent short circuits between two wound tapes. Therefore a performance of an electromagnet can be improved in the practical uses.

4. Conclusion

High temperature 0 %, 5 %, 8 % and 12 mole % Yb_2O_3-ZrO_2 insulation coatings were successfully produced on both sides of Ag substrates by the sol-gel process for magnet technologies. Turbidity values of Yb and Zr-based solutions including 0, 5, 8 and 12 % mole Yb were found to be 12.42, 4.24, 31.02 and 62.81 ntu, respectively. The pH values of the solutions were determined to be in the range of 2.81 and 4.05.

Taking into account a combination of DTA-TG, FTIR and XRD results, the optimum heating regime for this process was determined at temperatures such as 300°C for 10 minutes, 500°C for 5 minutes and 800°C for 60 minutes which respectively indicate combustion or drying, oxidation or heat treatment and annealing processes. The heat treated powders demonstrate several absoption bands at about 3300-3700 cm^{-1}, 2400-2700 cm^{-1}, 1400-1800 cm^{-1}, 900 cm^{-1} and 500 cm^{-1} corresponding to O-H, carboxyl and oxide groups. XRD patterns revealed that whilst ZrO_2 phase present in the structures with high intensity, Yb_3O_2 phase possessess low intensity peak. A regular surface morphology generally forms when Yb_2O_3 content increase in ZrO_2 from 0 mole % to 12 mole %.

The refractive indexes of 0 %, 5 %, 8 % and 12 mole % Yb_2O_3–ZrO_2 coatings annealed at 800°C were found in the range of 1.3539 and 1.3655. The film thicknesses of all coatings generally increased from 0.50 μm to 1.20 μm with increasing with number of dipping from 1 layer to 6 layers. Optical band gap values of 0 %, 5 %, 8 % and 12 mole % Yb_2O_3–ZrO_2 coatings annealed at 800°C are 3,0036 eV, 3,05166 eV, 3,02133 eV and 3,02836 eV, respectively. Empedance values of ZrO_2 and Yb_2O_3-ZrO_2 coatings were measured as 2.52 ohms and 2.51 ohms, respectively. Conductivity values of ZrO_2 and Yb_2O_3-ZrO_2 coatings were found to be 0.488 S/cm and 0.550 S/cm, respectively. Due to these reasons, after both sides of commercial Ag and AgMg sheathed Bi-2212 long length tapes are insulated with pure ZrO_2 and Yb_2O_3–ZrO_2 coatings, it can be

wound to fabricate an electromagnet.

References

Celik, E., Akın, Y., Sigmund W. and Hascicek, Y.S., 2003. High temperature Er$_2$O$_3$-ZrO$_2$ insulation coatings on Ag/AgMg sheathed Bi-2212 superconducting tapes via sol-gel technique. *IEEE Transactions on Applied Superconductivity,* **13**, 2988-2991.

Celik, E., Hascicek, Y.S. and Mutlu, I.H., 2002. High temperature compatible ınsulation for superconductors and method of applying ınsulation to superconductors. *USA Patent*, Patent number: **6,344,287 B1**.

Celik, E., Hascicek, Y.S. and Mutlu, I.H., 2002. Method of Applying High Temperature Compatible Insulation to Superconductors. USA Patent, Patent number: **6,387,852 B1**.

Celik, E. 2010. Ho$_2$O$_3$-ZrO$_2$ insulation coatings on AgMg sheathed Bi-2212 superconducting tapes by sol-gel technique for magnet technology. *J. Sol-gel Science and Technology,* **53,** 561-569.

Celik, E., Avci, E. and Hascicek, Y.S., 2004. Growth characteristic of ZrO$_2$ insulation coatings on Ag/AgMg sheathed Bi-2212 superconducting tapes. *Materials Science and Engineering B*, **110**, 213-220.

Ech-chamikh, E., Essafti, A., Azizan, M., Ijdiyaou, Y., 2006. Optical characterization of a-C:N thin films deposited by RF sputtering. *Solar Energy Materials and Solar Cells*, **90** 1424-1428.

Jerónimo, P.C.A., Araújo, A.N., Conceição, M. and Montenegro, B.S.M., 2004. Development of a sol–gel optical sensor for analysis of zinc in pharmaceuticals. *Sensors and Actuators B: Chemical*, **103**, 169-177.

Mutlu, I.H., Celik, E. and Hascicek, Y.S., 2002. High temperature ınsulation coatings and their electrical properties for HTS/LTS conductors. *Physica C*, **370**, 113–124.

Yue, Z., Guo, W., Zhou, J., Gui, Z., Li, L., 2004, Synthesis of nanocrystilline ferrites by sol–gel combustion process: the influence of pH value of solution. *J. Magnetism and Magnetic Materials*, **270**, 216-223.

Wilde, F.D. and Gibs, J., Geological Survey TWRI Book. 9, 1-30.

Weijers, H.W., Hu, Q.Y., Viouchkov, Y., Celik, E., Hascicek, Y.S., Marken, K., Parrell, J. and Schwartz, J., 2002. Development and testing of a 3 T Bi-2212 insert magnet. *Advances in Cryogenic Engineering (Materials)*, **45**, 769-778.